Capability of the PAMELA instrument to identify light-nuclei: results from a beam test calibration

R. Sparvoli [a], V. Malvezzi [a], L. Grishantseva [b], D. Campana [c], G. De Rosa [c], G. Osteria [c], W. Menn [d], L. Bonechi [e], M. Bongi [e], S. Ricciarini [e], E. Vannuccini [e]

a Dept. of Physics, University of Rome Tor Vergata and INFN, Rome (Italy)
b Moscow Engineering and Physics Institute, Moscow (Russia)
c Dept. of Physics, University of Naples and INFN, Naples (Italy)
d Dept. of Physics, University of Siegen, Siegen (Germany)
e Dept. of Physics, University of Florence and INFN, Florence (Italy)

Abstract— **PAMELA is a space telescope orbiting around the Earth since June 2006. The scientific objectives addresses by the mission are the measurement of the antiprotons and positrons spectra in cosmic rays, the hunt for anti-nuclei as well as the determination of light nuclei fluxes from hydrogen to oxygen in a wide energy range and with very high statistics.**
In this paper the charge discrimination capabilities of PAMELA for light nuclei, determined during a beam test calibration, will be presented.

I. INTRODUCTION

The PAMELA apparatus is designed to study charged particles in the cosmic radiation. It is hosted by a Russian Earth-observation satellite, the Resurs-DK1, that was launched into space by a Soyuz rocket on the 15th of June 2006 from the Baikonur cosmodrome. The orbit is elliptical and semi-polar, with an inclination of 70.0° and an altitude varying between 350 km and 600 km. The mission will last nominally three years. The main scientific goal of the experiment is the precise measurement of the cosmic-ray antiprotons and positrons energy spectra. The satellite orbit and mechanical design of the apparatus will allow the identification of these particles in an unprecedented energy range (between 50 MeV and 270 GeV for positrons and between 80 MeV and 190 GeV for antiprotons) and with high statistics (~10^4 antiprotons and ~ 10^5 positrons per year).
Additionally, PAMELA will search for antimatter in the cosmic radiation (sensitivity to the antiHe/He ratio of ~ 10^{-7}), it will investigate phenomena connected with Solar and Earth physics and will measure the light nuclear component of Galactic cosmic rays in the interval 80--200 MeV/n with an accuracy overcoming the uncertainties of the current propagation models.
The relative abundances of the constituents of Galactic cosmic rays provide information about cosmic-ray transport within the Galaxy. In particular, cosmic rays of primary origin such as Carbon, Nitrogen and Oxygen may interact with the interstellar medium to produce secondary fragments such as Lithium, Beryllium and Boron. The measured ratio of secondary to primary cosmic rays can be used to compute the mean amount of interstellar matter that cosmic rays have encountered before reaching the Earth, which ultimately provides important constraints on the composition and homogeneity of the ISM in which they propagate.
A better determination of the cosmic ray propagation is fundamental for the search of exotic matter, like dark matter candidates or antimatter produced in exotic processes, since the signature of such processes can be recognized only by knowing with great precision the fluxes due to the conventional production, acceleration and transport models [1].
The simplest GCR transport model, the leaky-box model (LBM), assumes a Galaxy with uniform density from which cosmic rays escape or ‘‘leak’’ out with an energy-dependent probability per unit time. More realistic models [2,3] account for the actual structure of the Galaxy, incorporating both a high-density central disk and a low-density halo. Recent models include the effects of cosmic-ray transport within the Local Bubble[4,5,6]. There are a number of recent reviews[7,8,9,10] of the cosmic-ray transport models and underlying computational techniques.
To clarify the role of the different mechanisms that act in the propagation of Galactic cosmic rays it is fundamental to have more precise and extended data on the secondary/primary abundance ratios (like the ratio B/C) and on the fluxes of primary particles: in this field PAMELA can represent a big step ahead.
Object of this paper is the presentation of the light-charge identification capabilities of PAMELA, as evaluated during a beam test performed at the GSI laboratory - Germany - in February 2006.

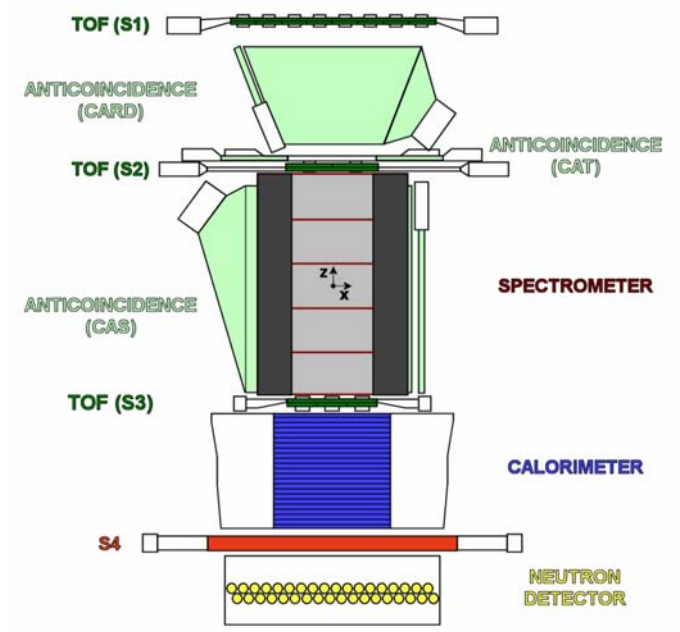

Figure 1: Sketch of the PAMELA instrument.

II. The instrument PAMELA

The PAMELA apparatus is composed by the following sub-detectors, arranged as in Figure 1, from top to bottom: a T*ime-of-Flight system* (TOF (S1,S2,S3)), an *anticoincidence system* (CARD, CAT, CAS), a *magnetic spectrometer*, an *electromagnetic imaging calorimeter*, a *shower tail catcher scintillator* (S4) and a *neutron detector*. Particles trigger the experiment via the main trigger provided by the TOF system, composed of 6 layers of segmented plastic scintillators arranged in three planes, or via additional triggers provided by the calorimeter and S4. The TOF system also measures the absolute value of the particles charge and flight time crossing its planes. In this way downgoing particles can be separated from upgoing ones. Furthermore, the acceptance of the apparatus can be varied by changing the configuration of the TOF layers used to form the trigger.
Particles not cleanly entering the PAMELA acceptance are rejected by the anticounter system. The rigidities of the particles are determined by the magnetic spectrometer, consisting of a permanent magnet and a silicon tracking system. Thus, positively and negatively charged particles can be identified. The final identification (i.e. positrons, electrons, antiprotons, etc.) is provided by the combination of the calorimeter and neutron detector information plus the velocity measurements from the TOF system at low momenta.
The detector is approximately 120 cm high, has a mass of about 470 kg and the power consumption is 355 W.
A daily amount of about 16 GByte of data recorded by the instrument is transmitted to ground. The main downlink center is located at the Research Center for Earth operative monitoring "NTs-OMZ" in Moscow (Russia); an average of 5--6 passages per day over the station allow PAMELA to download all scientific data along with telemetry data about the status of the detector (temperatures, power consumptions, voltage levels, ..).
A very detailed description of the PAMELA detector along with an overview of the entire mission can be found in [11].

TABLE I
BEAMS AVAILABLE AT THE GSI TEST

Particle	Energy (MeV/n)	Target	Angle (°)	Events
^{12}C	1200		0	269896
^{12}C	1200	×	0	123194
^{12}C	200		45	30378
^{12}C	200	×	45	196139
^{50}Cr	500		0	15976
^{50}Cr	500	×	0	173960
^{50}Cr	500	×	45	52241

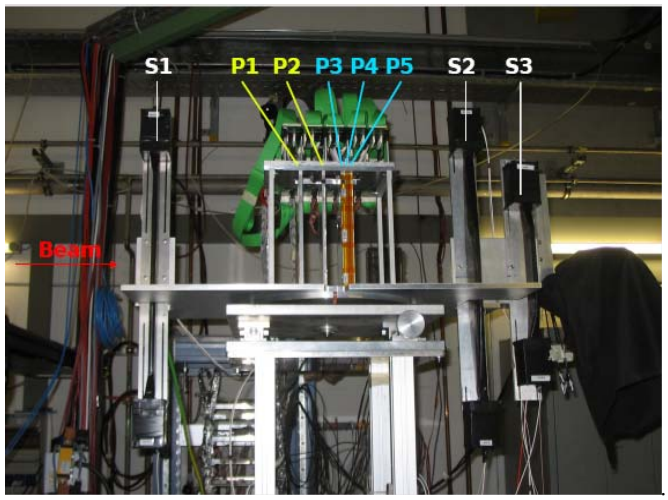

Figure 2: The experimental set-up of PAMELA at the GSI beam test.

III. GSI beam test

In its construction phase, PAMELA was exposed 3 times to beams of protons and electrons at the SPS/CERN accelerator, to study the performance of the detector with relativistic particles. Due to the tight schedule of PAMELA integration, however, there was no time for exposing it also to a light-nuclei beam, as sought. PAMELA flight model was delivered to Russia in March 2005.

Between the 16th and the 20th of February 2006 a prototype of the PAMELA Time-Of-Flight and silicon tracker were arranged in a mechanical frame and brought to the GSI (Gesellschaft für Schwerionenforschung, Darmstadt, Germany) beam accelerator. Figure 2 shows the arrangement of the instrument under test: only one paddle of every PAMELA TOF scintillator plane was used (indicated as S1, S2 and S3 in the picture), and a simpler version of the

PAMELA tracker, with only one silicon detector - for 5 planes - assembled (P1, P2, P3, P4 and P5 in figure).

The TOF paddles at GSI had the following dimensions: (40.8 x 5.5 x 0.7) cm^3 for S1, (18.0 x 7.5 x 0.5) cm^3 for S2 and (18.0 x 5.0 x 0.7) cm^3 for S3; the distance between S1 and S3 was the same as in PAMELA in flight, equal to about 80 cm [12]. The paddles were read out by two phototubes whose pulses were converted both in charge (ADC) and in time (TDC). This means that we had in total 6 signals for both ADC and TDC from the TOF detectors.

The TOF paddles performed also the fast trigger for the acquisition. The trigger configuration used was the AND between S1 and S2.

As for the tracker prototype, five non-equidistant 300 μm thick silicon detector planes were inserted into an aluminium frame. As for PAMELA, the double-sided silicon sensors (5.33×7.00) cm^2 provide two independent impact coordinates on each plane. Each high resistivity n-type silicon detector is segmented into micro-strips on both sides with p+ strips implanted on the junction side (bending-, x-view) and n+ strips on the Ohmic side (non-bending, y-view). In the x-view, the implantation pitch is 25 μm and the read-out pitch is 50 μm. In the y-view, the read-out pitch is 67 μm with the strips orthogonal to those in the x-view [13]. For every view we had a total of 1024 active micro-strips.

Principal aim of the test was to study the response of TOF and tracker at high-energy deposits, to observe when variations from linearity in the response of the electronics start to be visible. In addition, we wanted to study the charge resolution for light nuclei both for TOF and for tracker. Finally, of great interest was also the determination of the spatial resolution of the tracker for signals close to the saturation (as it is for Carbon): these results, however, will be published elsewhere.

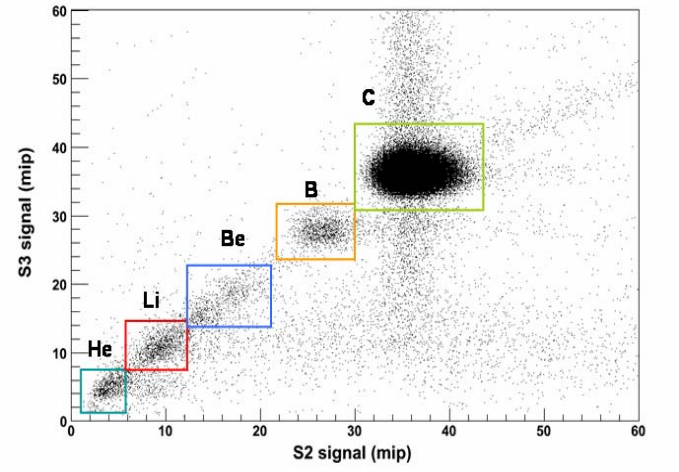

Figure 3: Scatter plot of the energy released in the S3 layer as a function of that in S2. Energies are expressed in mips. The different charge groups are visible.

Table 1 presents the beams available for the test. We had 3 primary beams of respectively ^{12}C at 1200 MeV/n, ^{12}C at 200 MeV/n and ^{50}Cr at 500 MeV/n. To produce secondaries, for some runs we used polyethylene and aluminium targets. To have more spread in energy, finally, in some acquisitions we rotated PAMELA at 45° with respect to the beam line to record only particles scattered at high angle.

Acquisition lasted 4 days, in a 24 hours/day cycle. During the day PAMELA was the main user of the beam, therefore it was possible to set the beam intensity to a most preferable value (about 1000 particles/spill, with spill duration of 4 s and time lap between spills of 3 s). During the night, instead, we were parasite of another experiment; the intensity was much higher (about 10^8 particles/spill) producing high statistics of acquisition but also a large amount of noise in the detector.

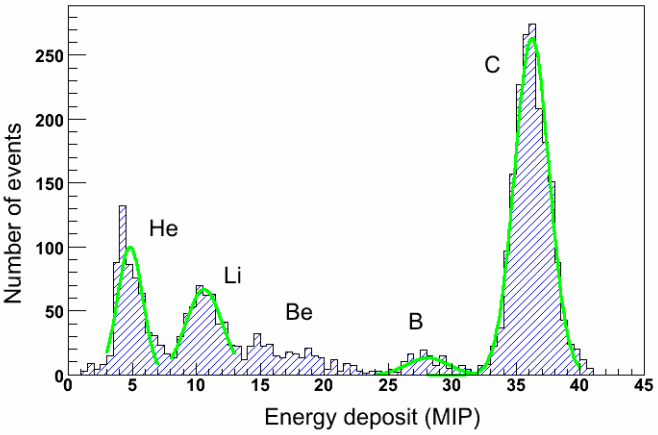

Figure 4: Histogram of the energy losses in the S3 layer of the TOF system. It is possible to see the different peaks corresponding to charges from He to C; a Gaussian fit, where possible, is superimposed to the peaks.

IV. Data analysis

To start the analysis we had to select clean particle tracks, without presence of double tracks (probable especially in the case of fragmented beams). In addition, we had to cut on possibly noisy or bad strips of the tracker, and noise signal on TOF scintillators.

More in detail, a "good" track inside the tracker was selected through the following requests:

- Elimination of noisy clusters along the track (a "cluster" is defined by one or more adjacent strips hit, with energy deposit 4 σ above the noise);
- Presence of only one cluster per view (to select single tracks);
- Presence of at least 3 views hit both in X and in Y, to perform a trajectory fit (we asked 3 views instead of 5 per view to account for the single layer inefficiency of the tracker, equal to about 10% for the prototype layers used at GSI);

- Consistency in the energy deposit in X and Y view, and along the track;
- Evaluation of a "good" linear fit in both views, estimated in terms of χ^2 of the fit.

As for the TOF, no special cuts have been applied, apart from those eliminating noise signals in the scintillators or wrong TDC values due to improper data unpacking for sporadic events.

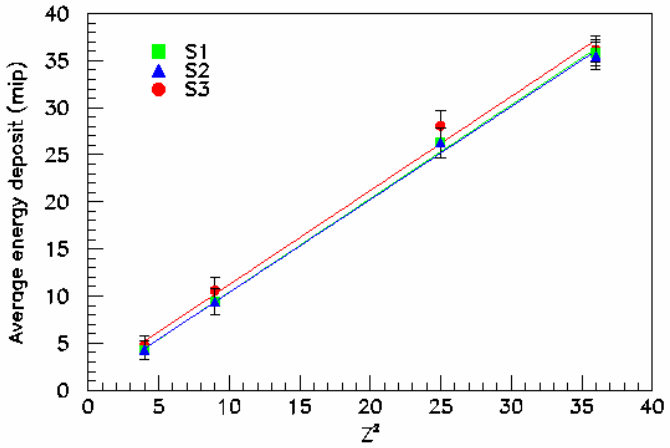

Figure 5: Behaviour of the energy deposit per paddle (S1, S2 and S3) as a function of Z^2. A linear fit is performed on the data. No loss of linearity is visible.

V. Response to Energy Releases

To study the response of the electronics we took the data of ^{12}C beam at 1200 MeV/n, with target. In this was we had a sample of different nuclei with an almost relativistic energy, and monochromatic.
We applied these aforementioned cuts on the data. In total, we remained with a sample of roughly 5000 events. Before proceeding with the analysis, we calibrated in mips (Minimum Ionizing Particle) both the energy deposit of TOF and tracker, by selecting either the initial Carbon beam or relativistic protons obtained by Carbon fragmentation.

A. Time-Of-Flight linearity

Figure 3 shows a scatter plot of the energy released in mips in the S2 and S3 layers for the sample of data under study. It is possible to see the regions corresponding to the different particle charges at different energies.
Figure 4 shows the histogram of the energy deposit in mips in the S3 scintillator. It is visible the presence of at least 5 peaks, corresponding to the fragmentation products of ^{12}C. Similar plots can be shown for S1 and S2. From the picture it is possible to see that relativistic protons are not visible; this is due to the fact that at the beam tests it was used an energy threshold for the ADC higher than that in flight, to study with greater detail the high energy deposits. The TDC threshold was instead kept at the same value as in flight, so relativistic protons could trigger the acquisition.

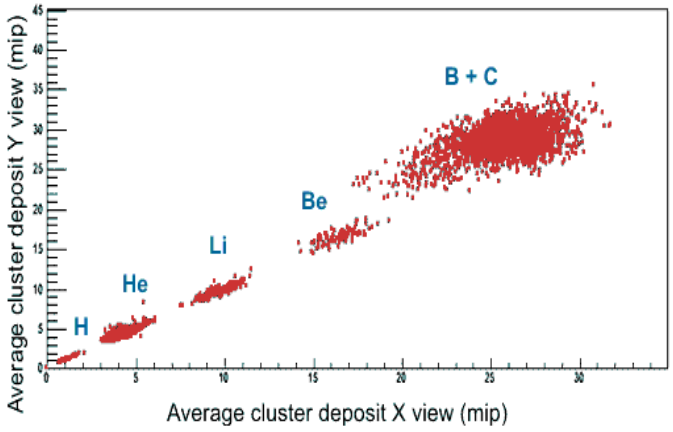

Figure 6: Average tracker cluster deposit in the Y view – in mips – versus that in the X view: the presence of group of events corresponding to the different charges is evident.

It is possible to try to perform Gaussian fits on the peaks visible in figure 3, and analogously for the deposit in S1 and S2, and evaluate the mean values of every fit. Figure 5 shows the behaviour of this mean value in S1, S2 and S3 as a function of Z^2. Errors on the mips deposits are given by the sigmas of the Gaussian distributions of the charge peaks of figure 4 (and similar for S1 and S2). Data fit very well with a linear curve, and no loss of linearity is visible up to Z=6.
To try to go beyond Carbon we studied the Chrome beam files. Unfortunately such beams saturated completely the TOF electronics; from the fragmentation products of the initial ^{50}Cr we could not get enough statistics to be able to study the TOF response to particles beyond Z=6.

B. Tracker linearity

The signals recorder in the silicon layers of the tracker are grouped in "cluster" structures, where a cluster is defined as one or more adjacent strips with a signal/noise ratio greater than 4 noise sigmas. Figure 6 shows the average cluster deposit in the Y view – in mips – versus that in the X view: the presence of group of events corresponding to the different charges is clearly shown.
Figure 7 shows the histogram of the single cluster energy deposit – in mips - averaged in the whole tracker. It is visible the presence of 5 peaks, corresponding to the fragmentation products of ^{12}C. The peaks of Carbon and Boron overlap, due to the saturation of the electronics.

Also in this case it is possible to perform Gaussian fits of the peaks, and evaluate the mean value of the fits. Figure 8 shows the behaviour of these energy values as a function of Z^2. Errors on the mips deposits are given by the sigmas of the Gaussian distributions of the peaks of figure 7. It is easy to see that, increasing the energy deposit over about 16 mips, the electronics starts to saturate. Data are no more fitted by a linear curve but rather by a polynomial function. The tracker

loss of linearity for high Z is not surprising since the tracker design was optimized for the detection of relativistic Z=1 particles, focused on the main scientific objectives of PAMELA. The read-out chips have indeed a nominal dynamic range of 10 mips.

The energy released by the Chrome beams, apart from clearly saturating the single channel deposit, created several levels of disturbance to the tracker electronics, therefore the ^{50}Cr acquisition files were discarded from the analysis.

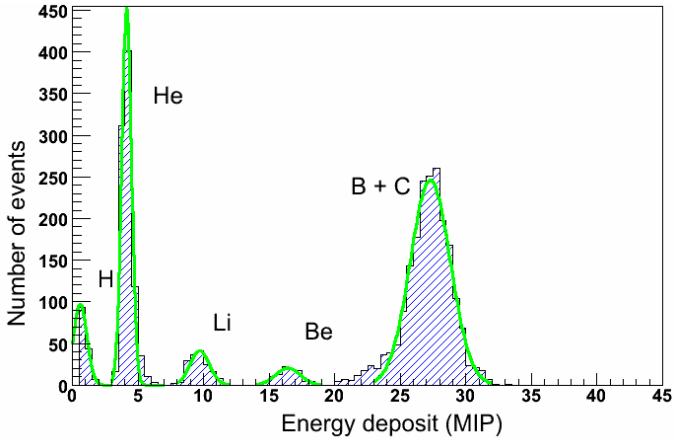

Figure 7: Average deposit per cluster in the tracker. The different charge peaks are visible. Carbon and Boron overlap, due to the saturation of the electronics.

VI. Charge resolution

To study the charge resolution of tracker and TOF we tried to have a data sample widely spread out in energy so to simulate as well as possible the situation in flight.
We have therefore taken the full statistics that was available for Carbon beams, namely the ^{12}C beam at 1200 MeV/n, with and without target, and the sample at 200 MeV/n, with and without target, and recorded at angles of both 0° and 45°.
First step of the charge identification process is the determination of the particle velocity. For straight particles the velocity β is obtained by inverting the following formula:

$$DS = K_1 + K_2 \frac{1}{\beta}$$

where ***DS*** is the difference of the sums of the two TDC counters of S3 and S1 [***DS*** = (TDC3_1 + TDC3_2) - (TDC1_1 - TDC1_2)] and K_1 and K_2 are two parameters that can be evaluated from the experimental data. For inclined particles or particles curved in a magnetic field it is necessary to evaluate the correct flight path. For the determination of the particle velocity it is possible to use also planes S1 and S2, but being the distance among them smaller the resolution in the reconstruction of β might be worse.
The width of the distribution of the reconstructed β determines the time resolution of the TOF, according to the simple relation $\Delta\beta = \beta c/L\ \Delta t$, being c the light speed and L the distance between the scintillators used to measure the velocity. Analysis of the measured β for straight ^{12}C beams at 1200 MeV/n, without target, has given the value of Δt = 62 ps as time resolution of the PAMELA TOF for light nuclei [14].

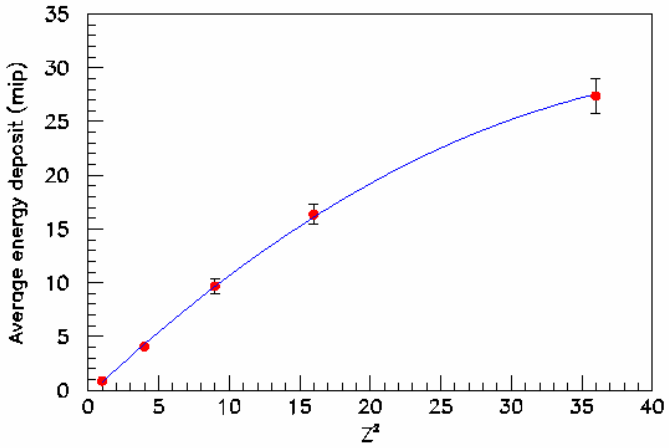

Figure 8: Behaviour of the average energy deposit per cluster as a function of Z^2. A polynomial fit is performed on the data. A loss of linearity is clearly visible above 16 mips.

A. TOF charge-identification

The charge is determined by the energy deposits in any of the three TOF planes in conjunction with the velocity measurement from the TOF, derived in our case by the top and the bottom scintillators. The three scintillator layers enable three independent charge determinations, thus improving significantly the charge resolution.
Figure 9 shows a plot of the energy loss *dE* in S2 as a function of the particle velocity β. We have chosen S2 because of the higher statistics for low energy light nuclei. Particles of

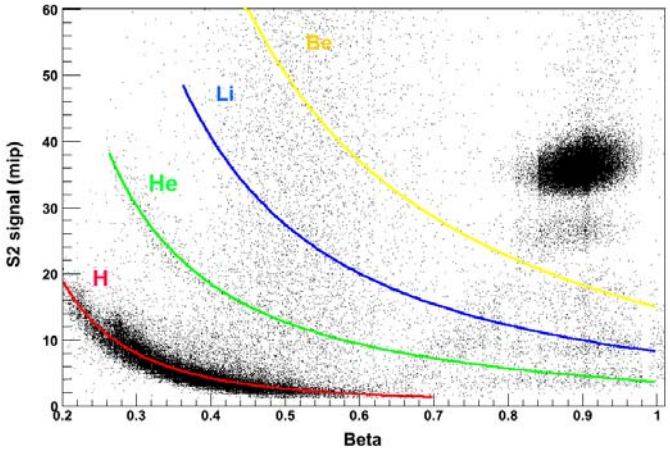

Figure 9: The energy deposit in S2 as a function of the measured velocity β. Particles fall into distinct charge bands that can be fitted by phenomenological functions.

different charge fall into distinct charge bands. Such bands can be fit, as shown by the curves superimposed to the points. A charge scale is then derived from the results of this fit.
In the ideal situation we should fit all charge bands so that particles fall between fitted curves. With the statistics collected at GSI, however, this was not possible and we could not clearly identify bands over Beryllium. The charge of particles heavier than Beryllium were then reconstructed by extrapolation from the existing charge bands.
Figure 10 shows the histogram of the charges in S2 reconstructed with this method. The charge peaks have been fitted by a Gaussian curve. Table 2 – second column - reports the values of the sigmas of the Gaussian fits. We can see that we reach the resolution of 0.15 units of charge for protons and 0.17 for carbon. The proton peak, made up only by non-relativistic protons, contains the contribution of deuterium and tritium not resolved. Same contribution of unresolved isotopes is present for Helium (He^3 and He^4 together), Lithium (Li^6 and Li^7), Beryllium (Be^7, Be^9 and Be^{10}) and Boron (B^{10} and B^{11}). Results presented in the second column of Table 2 have to be considered preliminary and are definitely upper limits, since additional corrections have still to be applied to the data. Such corrections include the effect of the attenuation of light along the scintillator paddle, and the time-walk correction.

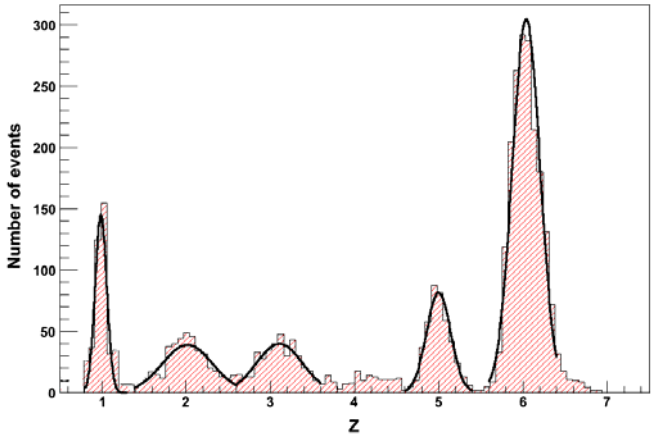

Figure 10: Charge resolution for particles at different beta and incident angle as measured by the TOF (plane S2). Where possible, Gaussian fits were superimposed to the data.

B. Tracker charge-identification

In analogy to what was done for the TOF, figure 11 shows a plot of the average energy loss per cluster *dE* in the tracker, as a function of the particle velocity β; only two curves (H and He) are clearly seen and can be fitted. Li and Be are not so abundant to allow a fitting of the charge band, and beyond starts the electronic saturation that overlaps charges.
Figure 12 presents the charge resolution obtained for the tracker, with superimposed – where possible – Gaussian fits for

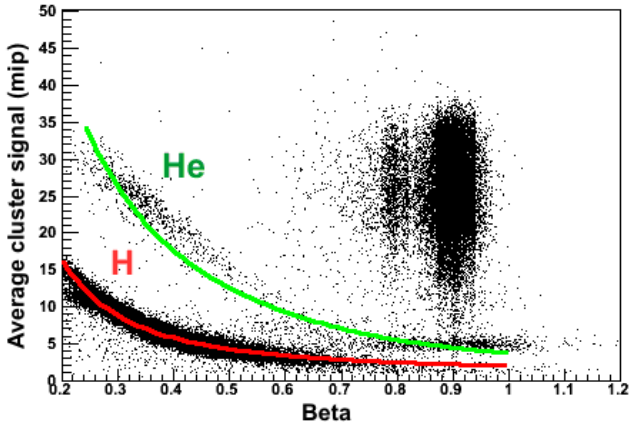

Figure 11: The average energy deposit in a tracker cluster as a function of the measured velocity β. Particles fall into distinct charge bands that can be fitted by phenomenological functions. In this case only the proton and helium bands are visible.

particles up to Helium. It is possible to see the different abundance of protons with respect to the same distribution seen from the TOF point of view, due to the abundant presence of relativistic protons cut away from the TOF ADC threshold.

Table 2 – third column - summarizes the results of tracker charge reconstruction in terms of the sigma of the Gaussian fits. It is possible to see the excellent results of charge resolution for Hydrogen and Helium. These resolutions have to considered as upper limits, since were obtained without applying corrections due to the electronics saturations, already present for the low-energy Helium component.

VII. RESULTS

The responses of tracker and TOF during the beam tests were not identical in terms of particle recognition. This was due to the fact that the sensitive area exposed to the beam was different for the two detectors. The scintillators area was bigger than the area of the silicon detectors, so particles scattered at relatively large angle might have been seen by the scintillators without crossing the tracker. This justifies partial differences seen in the particle abundances. In addition, as mentioned in section V, the TOF discriminating threshold in the ADC sector cut away relativistic protons from the TOF acquisition.
The analysis has shown that both tracker and TOF are able to discriminate light-charged particles. The tracker has an excellent charge discrimination for particles up to Helium, but beyond its performance degrades fast due to electronic saturation. The TOF has instead good charge resolution at least up to Z=6.

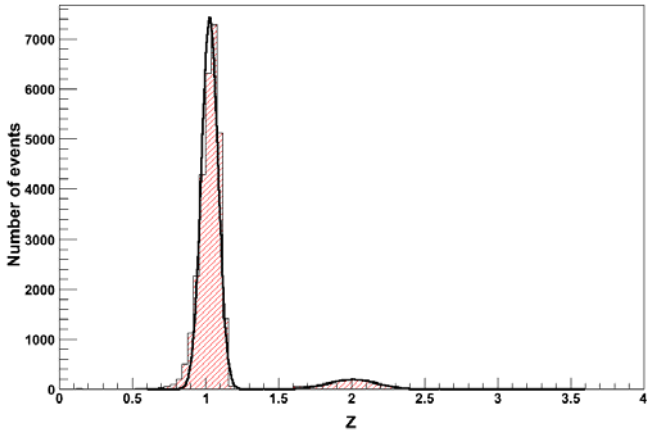

Figure 12: Charge resolution for Hydrogen and Helium at different beta and incident angle as measured by the tracker. Where possible, Gaussian fits were superimposed to the data.

Combining the information coming from the two detectors, thus square-summing the inverse of sigmas of second and third columns of Table 2, we can see that the charge resolution of PAMELA for light nuclei of different incoming energy goes from the value of 0.06 units of charge for protons up to around 0.17 for Carbon (see 4th column of the table). These results, which have to be considered preliminary since additional improvements can come from second order corrections to the data, are of the same order of magnitude of other space mission that measured nuclei and isotopes in the cosmic radiation, like the ISOMAX balloon-borne mission.

VIII. Conclusion

PAMELA is a space borne instrument flying in space since the 15th of June 2006. PAMELA will bring new measurements of the fluxes of antiprotons and positrons in an unexplored energy range, but also new important data about light-charged cosmic rays, thus helping understanding the transport and acceleration mechanisms of cosmic rays inside the Galaxy.

This paper has shown the capabilities of charge identification of PAMELA, as evaluated during a beam test of a prototype of the PAMELA TOF and tracker. Both TOF and tracker can reach a very good identification of light-nuclei, thanks to the information coming from the scintillators and the silicon wafers.

The capabilities of PAMELA in flight will be enriched by the presence of the imaging silicon calorimeter; every silicon layer of the calorimeter, indeed, as a dynamic range of about 1400 mips thus allowing even heavier charged particles to be recognized. Finally, PAMELA is a spectrometer equipped with a permanent magnet therefore also isotope recognition, at least for H and He, will be easily achieved.

TABLE II
PRELIMINARY CHARGE RESOLUTION FOR TOF, TRACKER AND COMBINED

PARTICLE (Z)	TOF RESOLUTION (σ)	TRACKER RESOLUTION (σ)	COMBINED RESOLUTION (σ)
1	0.15	0.06	0.06
2	0.31	0.16	0.14
3	0.27	-	0.17
5	0.14	-	0.14
6	0.17	-	0.17

ACKNOWLEDGMENT

We acknowledge the staff working at GSI, and especially dr. Dieter Schardt, for the excellent professionalism and friendly collaboration they offered us during the time in the laboratory.

REFERENCES

[1] D. Maurin et al., "Galactic Cosmic Ray Nuclei as a tool for Astroparticle Physics", astro-ph/0212111, to appear in Research Signposts "Recent Research Developments in Astrophysics".
[2] V. S. Prishchep & V. S. Ptuskin, Ap&SS, 1975, 32, p. 265.
[3] V. L. Ginzburg & V. S. Ptuskin, 1976, Rev. Mod. Phys, 48, p. 161.
[4] V. S. Ptuskin & A. Soutoul, 1998, A&A, 337, p. 859.
[5] I. V. Moskalenko & A. W. Strong, 2000, Ap&SS, 272, p. 247.
[6] R. E. Streitmatter & S. A. Stephens, 2001, Adv. Space Res., 27, p. 743.
[7] V. S. Berezinskii, 1990, Astrophysics of Cosmic Rays, ed. V. L. Ginzburg (Amsterdam: North-Holland).
[8] S. A. Stephens & R. E. Streitmatter, 1998, ApJ, 505, p. 266.
[9] M. Simon, 1999, in Topics in Cosmic-Ray Astrophysics, ed. M. DuVernois (Commack: Nova Science Publishers), p. 99.
[10] Moskalenko, I. V., et al. 2003, in Proc. 28th Int. Cosmic Ray Conf. (Tsukuba), 4, p. 1917.
[11] P. Picozza, A. M. Galper, G. Castellini et al., "PAMELA: a Payload for Antimatter Matter Exploration and Light-nuclei Astrophysics", astro-ph/ 0608697, submitted to Astroparticle Physics.
[12] G. Barbarino al, Nuclear Physics B, 2003, 125, p. 298.
[13] S. Straulino al, NIM A, 2004, 530, p. 168.
[14] G. Osteria al, "The ToF and Trigger systems of the PAMELA Experiment: performance of the flight model", this conference.